PHYSICAL REVIEW D **88,** 074012 (2013)

Process dependent nuclear $k_\perp$ broadening effect

Andreas Schäfer and Jian Zhou

Institut für Theoretische Physik, Universität Regensburg, Universitätsstraße 31, D-93053 Regensburg, Germany

(Received 16 June 2013; published 10 October 2013)

We study the process dependent nuclear $k_\perp$ broadening effect by employing the transverse momentum dependent (TMD) factorization approach in combination with the Mclerran-Venugopalan model. More specifically, we investigate how the parton transverse momentum distributions are affected by the process dependent gauge links in cold nuclear matter. In particular, our analysis also applies to the polarized cases including the nuclear quark Boer-Mulders function and the linearly polarized gluon distribution. Our main focus is on the nuclear TMDs at intermediate or large x.

DOI: 10.1103/PhysRevD.88.074012 PACS numbers: 13.85.−t, 13.88.+e

I. INTRODUCTION

The detailed understanding of the properties of hot and cold nuclear matter is one of the topical problems of QCD, in particular, in connection with high energy heavy-ion experiments at RHIC, LHC, and the future EIC. Initial/final state multiple parton rescattering in a large nucleus plays an important role in revealing the properties of cold nuclear matter, as it leads to various physical effects, such as transverse momentum broadening of the propagating parton, parton energy loss due to induced gluon bremsstrahlung, and nuclear dependence of azimuthal asymmetries.

Much efforts have been devoted to the study of transverse momentum broadening in eA and pA collisions. A number of different approaches developed to describe this phenomenon were formulated within different theoretical frameworks, such as the eikonal approximation [1], twist-4 collinear factorization [2] and the resummation of higher twist contributions [3,4], dipole approach [5,6], the BDMPS formalism [7–9], diagrammatic Glauber multiple scattering [10], color glass condensate effective theory [11,12], transverse momentum dependent factorization (TMD) [13], and soft collinear effective theory [14–17]. The energy dependence of nuclear $k_\perp$ broadening has also been investigated in Refs. [18,19].

Within the TMD factorization approach [20,21], we identified the gauge link appearing in the matrix element definition for nuclear TMDs as the main source of leading nuclear effects [13]. The formalism we developed in [13] was used to study $k_\perp$ broadening as well as the nuclear dependence of azimuthal asymmetries [22–24] in semi-inclusive DIS (SIDIS) off a large nucleus. In SIDIS nuclear TMDs contain a future-pointing gauge link describing the final state interactions, while a past-pointing gauge link shows up in the nuclear TMDs associated with the Drell-Yan process in pA collisions due to initial state interactions. The contributions to $k_\perp$ broadening from the future- and past-pointing gauge links are identical as this is a T-even observable. In the processes involving more complicated color flow, parton transverse momentum distributions can be affected by both initial and final state interactions, and thus could significantly differ from these in SIDIS and Drell-Yan (DY) processes. The initial/final state interactions leading to $k_\perp$ broadening in eA and pA collisions can be encoded in the various process dependent gauge links [25]. The purpose of this paper is to investigate the process dependent nuclear TMDs at intermediate or large x following our general method described in [13]. As a byproduct, one can readily deduce $k_\perp$ broadening simply by computing the $k_\perp^2$ moment of nuclear TMDs.

As a matter of fact, the process dependent nuclear TMDs at small x have been studied in both the unpolarized [26–28] and polarized cases [29,30]. In general, small x nuclear TMDs associated with different hard scattering processes recover the same well-known perturbative tail $1/k_\perp^2$ in the dilute medium limit, while they could differ significantly in the dense medium case where initial/final multiple rescattering plays a more important role for parton transverse momentum spectra. One remarkable example is the difference between two widely used small x gluon TMDs in saturation physics: the Weizsäcker-Williams (WW) gluon distributions and the dipole gluon distribution. As pointed out in [27,28], the WW gluon distribution contains a future- or past-pointing gauge link in the adjoint representation while the dipole distribution contains a closed loop gauge link. Both gluon distributions can be probed in different hard scattering processes [27,28].

In the present paper, we are aiming to extend the analyses [26–30] to the intermediate or large x region. At small x, TMDs are perturbatively calculable due to the presence of a semihard scale (the so-called saturation scale), generated dynamically in high energy scattering. In contrast, nuclear TMDs at intermediate or large x cannot be computed perturbatively. However, for the same reason, one can calculate contributions from initial/final state interactions encoded in process dependent gauge links in the Mclerran-Venugopalan (MV) model. By doing so, we are able to express nuclear TMDs as the convolution of the corresponding nucleon ones and process dependent small x gluon distributions. $k_\perp$ broadening is obtained as a byproduct from the relation between the nuclear TMD and the nucleon TMD in a specific hard scattering process.

At this point, we would like to briefly comment on the factorization properties of the relevant processes. Factorization in terms of TMDs containing process dependent gauge links is often referred to as generalized transverse momentum dependent (GTMD) factorization [25]. In the framework of GTMD factorization, the modified gauge links are obtained by resumming longitudinally polarized gluons into parton correlation functions on each nucleon side separately. However, recent work has shown that it is impossible to do so for dijet production in pp collisions because the initial/final state interaction will not allow a separation of gauge links into the matrix elements of the various TMDs associated with each incoming proton. This has been explicitly illustrated by a concrete counter-example in Ref. [31]. In pA collisions, if one only takes into account the interaction between the active partons and the background gluon field inside a large nucleus while neglecting the longitudinal gluons attached to the proton side, the type of graph (for example Fig. 11 in [31]) which can produce a violation of generalized TMD factorization disappears. After neglecting the extra gluon attachment on the proton side, multiple gluon rescattering between the hard part and the nucleus can be resummed to all orders in the form of a process dependent gauge link. As a result, the predictive power of the theory is partly restored in pA collisions.

We also noticed that the process dependent $k_\perp$ broadening effect has been studied within the twist-4 collinear factorization approach [32–34]. The fact that the twist-4 collinear approach can be applied in the intermediate and large x region allows us to directly compare our formalism with the high-twist approach. It is shown that two approaches yield identical physical results for $k_\perp$ broadening in different processes provided that the saturation scale and the twist-four quark gluon correlation functions are parametrized in a similar manner.

The paper is organized as follows. In Sec. II, we review our general method developed in [13] and apply a modified version to compute the nuclear enhancement of the transverse momentum imbalance for quark pair production in eA collisions and Drell-Yan dilepton production in pA collisions. In addition, we establish relations between nuclear quark Boer-Mulders distributions and nucleon ones in SIDIS and Drell-Yan using the same approach. In Sec. III, we study nuclear $k_\perp$ broadening for photon-jet production and quark pair production in pA collisions, respectively. In Sec. IV, we compare our results with those obtained in the collinear twist-4 approach and discuss the phenomenology implications. We conclude the paper and summarize our work in Sec. V.

II. NUCLEAR TMDS IN SIDIS AND DRELL-YAN PROCESSES

In our original work [13], multiple gluon correlations from the gauge link appearing in the definition of nuclear quark TMDs are reduced to products of nucleon small x gluon distribution in the so-called maximal two-gluon correlation approximation. From such expression, we obtained nuclear TMD as a convolution of a Gaussian distribution and a nucleon quark TMD. The width of the Gaussian is given by the gluon distribution density in the nuclear medium. However, the evaluation of Wilson lines in the MV model [35,36] has already reached a rather sophisticated level. In the present work, we will, therefore, compute the contribution from gauge links using the MV model instead of the maximal two-gluon correlation approximation. Both the unpolarized nuclear TMDs and the polarized TMDs (quark or gluon Boer-Mulders distributions) can be treated in the same framework. The resulting expression of the gauge link contribution in SIDIS computed in the MV model no longer has a Gaussian form once the finite nuclear matter size effect is taken into account. We start our derivation with the nuclear TMDs containing a simple future- or past-pointing gauge link.

A. Semi-inclusive DIS scattering off a large nucleus

In this subsection, we investigate how the outgoing quark transverse momentum spectrum is affected by final state interactions encoded in the future-pointing gauge link in the SIDIS process. The explicit relations between the nucleon quark TMDs and the corresponding nuclear ones are established.

Our starting point is the operator definition of quark TMDs in an unpolarized nucleon,

$$\begin{aligned}\mathcal{M}_N(x,\vec{k}_\perp) &= \int \frac{dr^- d^2 r_\perp}{(2\pi)^3} e^{ixP^+r^- - i\vec{k}_\perp\cdot\vec{r}_\perp}\langle N|\bar{\psi}(y^-,y_\perp)U^{[+]}\psi(r^-+y^-,r_\perp+y_\perp)|N\rangle \\ &= \frac{1}{2}f_{1,\mathrm{DIS}}(x,k_\perp)\not{p} + \frac{1}{2k_\perp}h^\perp_{1,\mathrm{DIS}}(x,k_\perp)\sigma^{\mu\nu}k_\mu p_\nu, \end{aligned} \tag{1}$$

where $k_\perp$ is defined as $k_\perp \equiv |\vec{k}_\perp|$, and p^μ is the commonly defined light cone vector. The average over coordinate y is implied. $|N\rangle$ represents the nucleon state. $f_{1,\mathrm{DIS}}(x,k_\perp)$ is the normal unpolarized quark distribution function containing a future-pointing gauge link which arises from the final state interaction in the semi-inclusive DIS process. The second parton distribution $h^\perp_{1,\mathrm{DIS}}(x,k_\perp)$ is commonly referred to as quark Boer-Mulders function [37]. Note that our convention for the quark Boer-Mulders function differs from the literature [38–40] by a factor $k_\perp/M_N$, where M_N is target mass. Roughly speaking, the quark Boer-Mulders function describes the strength of the correlation between

the quark transverse polarization and its transverse momentum. Color gauge invariance is ensured by two (future-pointing) gauge links in the fundamental representation,

$$U^{[+]} = \mathcal{P}e^{-ig\int_{y^-}^{\infty} d\zeta^- A^+(\zeta^-,y_\perp)}\mathcal{P}e^{-ig\int_{\infty}^{r^-+y^-} d\zeta^- A^+(\zeta^-,r_\perp+y_\perp)}. \tag{2}$$

We choose to work in the covariant gauge in which A^+ is the dominant component. The transverse pieces of the gauge link are suppressed and will be neglected in the derivation presented below [41].

Generally speaking, the longitudinal polarized gluons building up the gauge link may carry arbitrary collinear nucleon momentum fractions, since the gluon pole is not pinched. However, in this paper, we only focus on the contribution from small x gluons, which can be computed perturbatively due to the presence of a semihard scale Q_s. One might expect that the contribution to $k_\perp$ broadening from gluons with large (or intermediate) longitudinal momentum fraction is suppressed as compared to that from small x gluons because of the high gluon number density at small x and the larger transverse momentum carried by these gluons.

Following a standard procedure (see, e.g., Ref. [42] for an overview), one first solves the classical Yang-Mills equation and obtains

$$A_a^+(y^-,y_\perp) = -\frac{1}{\nabla_\perp^2}\rho_a(y^-,y_\perp), \tag{3}$$

where a is the color index. We proceed by inserting this solution into the gauge link and averaging over the color sources $\rho(x^-,x_\perp)$ with the Gaussian distribution $W[\rho]$ [35]:

$$W_A[\rho] = \exp\left\{-\frac{1}{2}\int d^3y \frac{\rho_a(y^-,y_\perp)\rho_a(y^-,y_\perp)}{\lambda_A(y^-)}\right\}, \tag{4}$$

where $\lambda_A(y^-)$ is the density of the color charges at a given y^-. With this ansatz for the distribution of color sources, the most elementary correlator is given by

$$\langle A_a^+(y^-,y_\perp)A_b^+(r^-,r_\perp)\rangle = \delta_{ab}\delta(y^- - r^-)\Gamma_A(y_\perp - r_\perp)\lambda_A(y^-) \qquad \Gamma_A(k_\perp) \equiv \frac{1}{k_\perp^4}. \tag{5}$$

By repeatedly using this elementary correlator, one evaluates a pair of Wilson lines stretching from $y^- + R^-$ to infinity with R^- being the nucleon radius,

$$\langle[\mathcal{P}e^{-ig\int_{y^-+R^-}^{\infty} d\zeta^- A^+(\zeta^-,y_\perp)}\mathcal{P}e^{-ig\int_{\infty}^{y^-+R^-} d\zeta^- A^+(r_\perp+y_\perp,\zeta^-)}]_{ab}\rangle = \exp\left\{-C_F\Theta(r_\perp^2)\int_{R^-+y^-}^{\infty} d\zeta^-\lambda_A(\zeta^-)\right\}\delta_{ab}, \tag{6}$$

where $\Theta(r_\perp^2) \equiv g^2[\Gamma_A(0_\perp) - \Gamma_A(r_\perp)] \simeq g^2\frac{r_\perp^2}{16\pi}\ln\frac{1}{r_\perp^2\Lambda_{\rm QCD}^2}$. Note that these two Wilson lines are connected in color space at infinity. The resulting expression is a production of the unitary color matrix and an exponential. This procedure is illustrated in Fig. 1.

Inserting this expression into the matrix element $\mathcal{M}_N$, one obtains,

$$\mathcal{M}_N(x,\vec{k}_\perp) = \int\frac{dr^-d^2r_\perp}{(2\pi)^3}e^{ixP^+r^- - i\vec{k}_\perp\cdot\vec{r}_\perp}\langle N|\bar{\psi}(y^-,y_\perp)\bar{U}^{[+]}\psi(r^-+y^-,r_\perp+y_\perp)|N\rangle\exp\left\{-C_F\Theta(r_\perp^2)\int_{R^-+y^-}^{\infty} d\zeta^-\lambda_A(\zeta^-)\right\}. \tag{7}$$

Here, the gauge link $\bar{U}^{[+]}$ is a short one and defined as

$$\bar{U}^{[+]} = \mathcal{P}e^{-ig\int_{y^-}^{R^-+y^-} d\zeta^- A^+(\zeta^-,y_\perp)}\mathcal{P}e^{-ig\int_{R^-+y^-}^{r^-+y^-} d\zeta^- A^+(\zeta^-,r_\perp+y_\perp)}, \tag{8}$$

which consists of two short Wilson lines connected in color space at point $R^- + y^-$. Apparently, the density of the color sources outside a nucleon is zero: $\int_{R^-+y^-}^{\infty} d\zeta^-\lambda_A(\zeta^-) = 0$. Such a vanishing contribution from the gauge link outside a nucleon has also been clearly seen in the lattice calculation [43]. As a result, the exponential factor in Eq. (7) becomes unity. The TMD correlator is reduced to

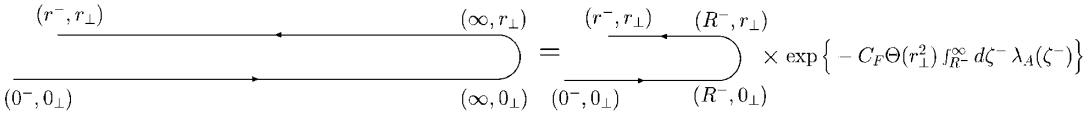

FIG. 1. The ordinary future-pointing gauge link is reduced to a short one by evaluating part of the gauge link stretching from R^- to ∞ in the MV model, where R^- is the radius of a nucleon.

$$\mathcal{M}_N(x,\vec{k}_\perp) = \int \frac{dr^- d^2 r_\perp}{(2\pi)^3} e^{ixP^+r^- - i\vec{k}_\perp\cdot\vec{r}_\perp} \langle N|\bar{\psi}(0^-,0\ \perp)\bar{U}^{[+]}\psi(r^-,r_\perp)|N\rangle$$
$$= \frac{1}{2} f_{1,\mathrm{DIS}}(x,k_\perp)\not{p} + \frac{1}{2k_\perp} h^\perp_{1,\mathrm{DIS}}(x,k_\perp)\sigma^{\mu\nu}k_\mu p_\nu, \tag{9}$$

where we have shifted the coordinate y to zero using translation invariance.

Note that the above derivation applies to both nuclear and nucleon targets and that all results have the same form. The only difference is that for a large nucleus target, the struck nucleon is surrounded by cold nuclear matter, such that the density of color sources outside the struck nucleon is no longer zero. Here, we further assume that the hadronization process takes place outside the nucleus,

$$\mathcal{M}_A(x,\vec{k}_\perp) = \int \frac{dr^- d^2 r_\perp}{(2\pi)^3} e^{ixP^+r^- - i\vec{k}_\perp\cdot\vec{r}_\perp} \langle A|\bar{\psi}(y^-,y_\perp)\bar{U}^{[+]}\psi(r^-+y^-,r_\perp+y_\perp)|A\rangle \exp\left\{-C_F\Theta(r_\perp^2)\int_{R^-+y^-}^\infty d\zeta^-\lambda_A(\zeta^-)\right\}$$
$$= \frac{1}{2}\mathbf{f}_{1,\mathrm{DIS}}(x,k_\perp)\not{p} + \frac{1}{2k_\perp}\mathbf{h}^\perp_{1,\mathrm{DIS}}(x,k_\perp)\sigma^{\mu\nu}k_\mu p_\nu, \tag{10}$$

where $\mathbf{f}_{1,\mathrm{DIS}}$ and $\mathbf{h}^\perp_{1,\mathrm{DIS}}$ denote the unpolarized quark and quark Boer-Mulders TMD distributions inside a large nucleus, respectively. To proceed further, we make two assumptions:

(1) we neglect the correlation between different nucleons and assume the large nucleus as a weakly bound,

$$\langle A|\bar{\psi}(y^-,y_\perp)\bar{U}^{[+]}\psi(r^-+y^-,r_\perp+y_\perp)|A\rangle = \langle N|\bar{\psi}(0^-,0_\perp)\bar{U}^{[+]}\psi(r^-,r_\perp)|N\rangle \int dy^- d^2y_\perp \rho_N^A(y), \tag{11}$$

where $|N\rangle$ is understood as the nucleon state averaged over protons and neutrons inside a large nucleus, and $\rho_N^A(y)$ is the spatial nucleon density normalized to the atomic number $\mathcal{A}$;

(2) we further describe the large nucleus as a homogenous system of nucleons and color sources,

$$\rho_N^A(y) = \rho_N^A(0), \qquad \lambda_A(\zeta^-) = \lambda_A(0^-). \tag{12}$$

Implementing these two approximations, one has

$$\mathcal{M}_A(x,\vec{k}_\perp) = \int \frac{dr^- d^2 r_\perp}{(2\pi)^3} e^{ixP^+r^- - i\vec{k}_\perp\cdot\vec{r}_\perp} \langle N|\bar{\psi}(0^-,0_\perp)\bar{U}^{[+]}\psi(r^-,r_\perp)|N\rangle$$
$$\times \int dy^- d^2y_\perp \rho_N^A(y^-)\exp\left\{-C_F\Theta(r_\perp^2)\int_{R^-+y^-}^\infty d\zeta^-\lambda_A(\zeta^-)\right\}$$
$$\approx \mathcal{A}\int \frac{dr^- d^2 r_\perp}{(2\pi)^3} e^{ixP^+r^- - i\vec{k}_\perp\cdot\vec{r}_\perp} \langle N|\bar{\psi}(0^-,0_\perp)\bar{U}^{[+]}\psi(r^-,r_\perp)|N\rangle \frac{1-e^{-\frac{r_\perp^2 Q_{s,q}^2}{4}}}{r_\perp^2 Q_{s,q}^2/4}. \tag{13}$$

In the second step of the above equation, the approximation $\int_{R^-+y^-}^\infty d\zeta^-\lambda_A(\zeta^-) \approx \int_{y^-}^\infty d\zeta^-\lambda_A(\zeta^-)$ valid for a large nucleus target has been used. The quark saturation momentum $Q_{s,q}$ is given by $Q_{s,q}^2 = \alpha_s C_F \ln\frac{1}{r_\perp^2\Lambda_{\mathrm{QCD}}^2}\int_{-\infty}^\infty d\zeta^-\lambda_A(\zeta^-)$.

Equation (13) can be reexpressed in momentum space as

$$\mathcal{M}_A(x,\vec{k}_\perp) = \mathcal{A}\int d^2l_\perp \mathcal{M}_N(x,\vec{l}_\perp)\mathcal{F}_{\mathrm{DIS}}(|\vec{k}_\perp - \vec{l}_\perp|). \tag{14}$$

Here $\mathcal{F}_{\mathrm{DIS}}(|\vec{k}_\perp - \vec{l}_\perp|)$ is given by

$$\mathcal{F}_{\mathrm{DIS}}(|\vec{k}_\perp - \vec{l}_\perp|) = \int \frac{d^2r_\perp}{(2\pi)^2} e^{-i(\vec{k}_\perp-\vec{l}_\perp)\cdot\vec{r}_\perp} 4\frac{1-e^{-\frac{r_\perp^2 Q_{s,q}^2}{4}}}{r_\perp^2 Q_{s,q}^2}, \tag{15}$$

and is normalized to 1: $\int d^2l_\perp \mathcal{F}_{\mathrm{DIS}}(l_\perp) = 1$. When $Q_{s,q}^2$ is small, the fact that $\mathcal{F}_{\mathrm{DIS}}(|\vec{k}_\perp - \vec{l}_\perp|) \simeq \delta^2(\vec{k}_\perp - \vec{l}_\perp)$ allows us to recover the usual nucleon TMDs. Inserting the decomposition of the matrix correlator into Eq. (14), it is easy to derive that

$$\mathbf{f}_{1,\mathrm{DIS}}(x,k_\perp) = \mathcal{A}\int d^2l_\perp f_{1,\mathrm{DIS}}(x,l_\perp)\mathcal{F}_{\mathrm{DIS}}(|\vec{k}_\perp-\vec{l}_\perp|) \tag{16}$$

$$\mathbf{h}^\perp_{1,\mathrm{DIS}}(x,k_\perp) = \mathcal{A}\int d^2l_\perp(\hat{k}_\perp\cdot\hat{l}_\perp)h^\perp_{1,\mathrm{DIS}}(x,l_\perp)\mathcal{F}_{\mathrm{DIS}}(|\vec{k}_\perp-\vec{l}_\perp|). \tag{17}$$

The unit vectors $\hat{k}_\perp$ and $\hat{l}_\perp$ are defined as $\hat{k}_\perp \equiv \vec{k}_\perp/k_\perp$ and $\hat{l}_\perp \equiv \vec{l}_\perp/l_\perp$, respectively. From these relations between nucleon TMDs and nuclear TMDs, one finds,

$$\int d^2k_\perp \mathbf{f}_{1,\mathrm{DIS}}(x,k_\perp) = \mathcal{A}\int d^2l_\perp f_{1,\mathrm{DIS}}(x,l_\perp) = \mathcal{A}f_1(x), \tag{18}$$

$$\int d^2k_\perp k_\perp^2 \mathbf{f}_{1,\mathrm{DIS}}(x,k_\perp) = \mathcal{A}\int d^2l_\perp l_\perp^2 f_{1,\mathrm{DIS}}(x,l_\perp) + \frac{1}{2}Q_{s,q}^2\mathcal{A}f_1(x), \tag{19}$$

$$\int d^2k_\perp k_\perp \mathbf{h}^\perp_{1,\mathrm{DIS}}(x,k_\perp) = \mathcal{A}\int d^2l_\perp l_\perp h^\perp_{1,\mathrm{DIS}}(x,l_\perp) = -2\pi M_N\mathcal{A}T_F^{(\sigma)}(x,x). \tag{20}$$

$f_1(x)$ is the normal integrated unpolarized quark distribution of a nucleon, while $T_F^{(\sigma)}(x,x)$ (convention used in Refs. [38,39]) is the twist-3 quark gluon correlation function inside an unpolarized nucleon. In the last step of Eq. (20), we used the well-known relation between the moment of the Boer-Mulders function and $T_F^{(\sigma)}(x,x)$ [44]. It turns out that this relation is not affected by the cold nuclear medium. Moreover, for the approximations made in this paper, the unpolarized quarks inside a large nucleus are redistributed in transverse momentum space while the total probability to find a quark carrying a certain longitudinal momentum fraction x remains unchanged. To be more specific, the quark transverse momentum distribution becomes broader and the transverse momentum broadening squared is $Q_{s,q}^2/2$.

In the semihard region where $k_\perp^2$ is of the order $Q_{s,q}^2$, Eqs. (16) and (17) can be simplified by dropping the terms suppressed by powers $\langle l_\perp^2\rangle/Q_{s,q}^2$ where $\langle l_\perp^2\rangle$ is the average squared parton intrinsic transverse momentum inside a nucleon,

$$\mathbf{f}_{1,\mathrm{DIS}}(x,k_\perp) \simeq \mathcal{A}f_1(x)\mathcal{F}_{\mathrm{DIS}}(k_\perp), \tag{21}$$

$$\mathbf{h}^\perp_{1,\mathrm{DIS}}(x,k_\perp) \simeq \mathcal{A}2\pi M_N T_F^{(\sigma)}(x,x)\frac{1}{2}\frac{\partial\mathcal{F}_{\mathrm{DIS}}(k_\perp)}{\partial k_\perp}, \tag{22}$$

which is the main result of this section. We believe that the main feature of multiple scattering in the cold nuclear matter has been captured in the above equations though various approximations were made in deriving them.

We conclude this subsection by emphasizing again the important point that the derivation presented above is only valid for nuclear TMDs at intermediate x or large x. In our calculation, it was critical to assume that the hard scattering takes place locally inside a nucleon, i.e., $r^- \le R^-$. This is in sharp contrast to the dipole model where the quark-antiquark pair coherently interacts with the whole nucleus.

B. The Drell-Yan process in pA collisions

We now turn to $k_\perp$ broadening in the Drell-Yan process. In a widely used hybrid approach (for a review, see [45]), one utilizes ordinary integrated parton distributions for the dilute projectile proton, while the transverse momentum carried by a parton coming from a nucleus is left unintegrated. We adopted the same strategy when dealing with pA collisions throughout this paper. As a consequence, at lowest order, the obtained transverse momentum spectrum of the produced virtual photon is directly related to the $k_\perp^2$ moment of the nuclear quark TMDs.

Quark TMDs appearing in Drell-Yan differential cross sections contain a past-pointing gauge link,

$$U^{[-]} = \mathcal{P}e^{-ig\int_{y^-}^{-\infty}d\zeta^- A^+(\zeta^-,y_\perp)}\mathcal{P}e^{-ig\int_{-\infty}^{r^-+y^-}d\zeta^- A^+(\zeta^-,r_\perp+y_\perp)}. \tag{23}$$

Following the procedure outlined in the previous subsection, one obtains the same relations between nucleon quark TMDs and nuclear quark TMDs,

$$\mathbf{f}_{1,\mathrm{DY}}(x,k_\perp) = \mathcal{A}\int d^2l_\perp f_{1,\mathrm{DY}}(x,l_\perp)\mathcal{F}_{\mathrm{DY}}(|\vec{k}_\perp-\vec{l}_\perp|), \tag{24}$$

$$\mathbf{h}^\perp_{1,\mathrm{DY}}(x,k_\perp) = \mathcal{A}\int d^2l_\perp(\hat{k}_\perp\cdot\hat{l}_\perp)h^\perp_{1,\mathrm{DY}}(x,l_\perp)\mathcal{F}_{\mathrm{DY}}(|\vec{k}_\perp-\vec{l}_\perp|), \tag{25}$$

with

$$\mathcal{F}_{\mathrm{DY}}(|\vec{k}_\perp-\vec{l}_\perp|) = \mathcal{F}_{\mathrm{DIS}}(|\vec{k}_\perp-\vec{l}_\perp|). \tag{26}$$

Similarly, a shorter past-pointing gauge link emerges in the matrix element definition for $f_{1,\mathrm{DY}}(x,l_\perp)$ and $h^\perp_{1,\mathrm{DY}}(x,l_\perp)$,

$$\bar{U}^{[-]} = \mathcal{P} e^{-ig\int_0^{-R^-} d\zeta^- A^+(\zeta^-,0_\perp)} \mathcal{P} e^{-ig\int_{-R^-}^{r^-} d\zeta^- A^+(\zeta^-,r_\perp)}. \tag{27}$$

In the above formula, the coordinate y has again been shifted to zero by translation invariance. With this shorter gauge link, using time reversal and parity invariance, one may readily deduce,

$$\begin{aligned} f_{1,\mathrm{DY}}(x, l_\perp) &= f_{1,\mathrm{DIS}}(x, l_\perp), \\ h^\perp_{1,\mathrm{DY}}(x, l_\perp) &= -h^\perp_{1,\mathrm{DIS}}(x, l_\perp), \end{aligned} \tag{28}$$

and therefore,

$$\begin{aligned} \mathbf{f}_{1,\mathrm{DY}}(x, l_\perp) &= \mathbf{f}_{1,\mathrm{DIS}}(x, l_\perp), \\ \mathbf{h}^\perp_{1,\mathrm{DY}}(x, l_\perp) &= -\mathbf{h}^\perp_{1,\mathrm{DIS}}(x, l_\perp). \end{aligned} \tag{29}$$

We notice that the unique universality property of the T-odd distribution $\mathbf{h}^\perp_1$ [46,47] is preserved under our manipulation of gauge links. In the end, we would like to mention that the transverse momentum broadening for a virtual photon produced in pA collisions is also parametrized by $Q^2_{s,q}/2$.

C. Heavy quark pair production in eA collisions

We study the nuclear broadening of heavy quark-antiquark pair momentum imbalance in eA collisions. Heavy quark production in eA collisions is initiated by the gluon channel,

$$\gamma^* + g \to Q + \bar{Q}. \tag{30}$$

The transverse momentum imbalance of a quark-antiquark pair is defined as

$$\vec{k}_\perp = \vec{p}_{1\perp} + \vec{p}_{2\perp}, \tag{31}$$

where $\vec{p}_{1\perp}$ and $\vec{p}_{2\perp}$ are the transverse momenta of the produced quark and antiquark, respectively. In TMD factorization and at leading order, $\vec{k}_\perp$ is identical to the transverse momentum carried by the incoming gluon simply because of momentum conservation. The matrix element definition for nuclear gluon TMDs in SIDIS is given in [48,49]

$$\begin{aligned} \mathcal{M}^{ij}_A(x, \vec{k}_\perp) &= \int \frac{dr^- d^2 r_\perp}{(2\pi)^3 P^+} e^{ixP^+ r^- - i\vec{k}_\perp\cdot\vec{r}_\perp} \langle A|F^{+i}(y^-, y_\perp)\tilde{U}^{[+]} L_y F^{+j}(r^- + y^-, r_\perp + y_\perp)|A\rangle \\ &= \frac{\delta^{ij}_\perp}{2} x\mathbf{G}_{\mathrm{DIS}}(x, k_\perp) + \left(\hat{k}^i_\perp \hat{k}^j_\perp - \frac{1}{2}\delta^{ij}_\perp\right) x\mathbf{h}^{\perp g}_{1,\mathrm{DIS}}(x, k_\perp), \end{aligned} \tag{32}$$

where $\tilde{U}^{[+]}$ is the future-pointing gauge link in the adjoint representation. $\mathbf{G}_{\mathrm{DIS}}$ and $\mathbf{h}^{\perp g}_{1,\mathrm{DIS}}$ stand for the unpolarized gluon TMD and linearly polarized gluon TMD, respectively. $\mathbf{h}^{\perp g}_{1,\mathrm{DIS}}$ is the only polarization dependent gluon TMD for an unpolarized nucleon/nucleus, and therefore may be considered as the counterpart of the quark Boer-Mulders function. However, in contrast to the later, $\mathbf{h}^{\perp g}_{1,\mathrm{DIS}}$ is a time-reversal even distribution, implying $\mathbf{h}^{\perp g}_{1,\mathrm{DIS}} = \mathbf{h}^{\perp g}_{1,\mathrm{DY}}$. The linearly polarized gluon distribution inside a large nucleus recently attracted a lot of attentions. $\mathbf{h}^{\perp g}$ in the saturation regime was first derived using the MV model in [29]. Its rapidity evolution was also investigated [50]. Many processes in which $\mathbf{h}^{\perp g}$ can be probed have been proposed [29,30,50–52].

It is straightforward to extend our analysis for nuclear quark TMDs to gluon TMDs. One thus obtains

$$\mathbf{G}_{\mathrm{DIS}}(x, k_\perp) = \mathcal{A}\int d^2 l_\perp G_{\mathrm{DIS}}(x, l_\perp)\mathcal{F}^g_{\mathrm{DIS}}(|\vec{k}_\perp - \vec{l}_\perp|), \tag{33}$$

$$\begin{aligned} \mathbf{h}^{\perp g}_{1,\mathrm{DIS}}(x, k_\perp) = \mathcal{A}\int d^2 l_\perp [2(\hat{k}_\perp\cdot\hat{l}_\perp)^2 - 1] h^{\perp g}_{1,\mathrm{DIS}}(x, l_\perp) \\ \times \mathcal{F}^g_{\mathrm{DIS}}(|\vec{k}_\perp - \vec{l}_\perp|). \end{aligned} \tag{34}$$

G_{DIS} and $h^{\perp g}_{1,\mathrm{DIS}}$ are corresponding gluon distributions in a nucleon. $\mathcal{F}^g_{\mathrm{DIS}}(|\vec{k}_\perp - \vec{l}_\perp|)$ is given by

$$\mathcal{F}^g_{\mathrm{DIS}}(|\vec{k}_\perp - \vec{l}_\perp|) = \int \frac{d^2 r_\perp}{(2\pi)^2} e^{-i(\vec{k}_\perp - \vec{l}_\perp)\cdot\vec{r}_\perp} 4\frac{1 - e^{-\frac{r^2_\perp Q^2_s}{4}}}{r^2_\perp Q^2_s}, \tag{35}$$

where $Q^2_s = \alpha_s N_c \ln\frac{1}{r^2_\perp \Lambda^2_{\mathrm{QCD}}} \int_{-\infty}^{\infty} d\zeta^- \lambda_A(\zeta^-)$ is the gluon saturation momentum. With these relations, it is easy to further verify that

$$\begin{aligned} &\int d^2 k_\perp k^2_\perp \mathbf{G}_{\mathrm{DIS}}(x, k_\perp) \\ &\quad = \mathcal{A}\int d^2 l_\perp l^2_\perp G_{\mathrm{DIS}}(x, l_\perp) + \frac{1}{2} Q^2_s \mathcal{A} G_{\mathrm{DIS}}(x), \end{aligned} \tag{36}$$

$$\int d^2 k_\perp k^2_\perp \mathbf{h}^{\perp g}_{1,\mathrm{DIS}}(x, k_\perp) = \mathcal{A}\int d^2 l_\perp l^2_\perp h^{\perp g}_{1,\mathrm{DIS}}(x, l_\perp). \tag{37}$$

Correspondingly, the quark-antiquark momentum imbalance in eA collisions is again of order $Q^2_s/2$.

III. NUCLEAR TMDs IN PHOTON-JET AND HEAVY QUARK PAIR PRODUCTION IN pA COLLISIONS

When both initial and final state interactions are present in a hard scattering, a more complicated structure of gauge links different from simple past- or future-pointing ones will appear. This results in the process dependent nuclear $k_\perp$ broadening.

A. Nuclear TMDs in photon-jet production

We first study the nuclear enhancement of the transverse momentum imbalance for photon-jet production in pA collisions,

$$p(P') + A(P) \to \gamma(p_1) + \mathrm{Jet}(p_2) + X, \tag{38}$$

where P' and P are the momenta of incoming proton and nucleus (per nucleon), and p_1, p_2 are the momenta of the produced photon and jet, respectively. The transverse momentum imbalance $\vec{q}_\perp$ is defined as $\vec{q}_\perp = \vec{p}_{1\perp} + \vec{p}_{2\perp}$.

For the $q\bar{q} \to \gamma g$ channel, the corresponding gauge link is built up by both initial state and final state interactions. The resulting nuclear quark TMDs are give by [25]

$$\begin{aligned}\mathcal{M}_A(x,\vec{k}_\perp) &= \int \frac{dr^- d^2r_\perp}{(2\pi)^3} e^{ixP^+r^- - i\vec{k}_\perp\cdot\vec{r}_\perp}\langle A|\bar{\psi}(y^-,y_\perp)\left\{\frac{9}{8N_c}U^{[+]}\mathrm{Tr}_c[U^{[\Box]\dagger}] - \frac{1}{8}U^{[-]}\right\}\psi(r^- + y^-, r_\perp + y_\perp)|A\rangle \\ &= \frac{1}{2}\mathbf{f}_{1,q\bar{q}\to\gamma g}(x,k_\perp)\not{p} + \frac{1}{2k_\perp}\mathbf{h}^\perp_{1,q\bar{q}\to\gamma g}(x,k_\perp)\sigma^{\mu\nu}k_\mu p_\nu,\end{aligned} \tag{39}$$

where $U^{[\Box]} = U^{[+]}U^{[-]\dagger} = U^{[-]\dagger}U^{[+]}$ emerges as a Wilson loop. The technique for evaluating multiple point correlation functions in the MV model has been systematically developed in Ref. [53]. The main strategy is to repeatedly use the Fierz identity $t^a_{ij}t^a_{kl} = \frac{1}{2}\delta_{il}\delta_{jk} - \frac{1}{2N_c}\delta_{ij}\delta_{kl}$ in order to resolve the color structure when gluon links connect different gauge links. By closely following the method presented in [53], we compute part of the gauge link $U^{[+]}U^{[+]\dagger}$ in the MV model,

$$\begin{aligned}&\langle[\mathcal{P}e^{-ig\int_{y^-+R^-}^{\infty}d\zeta^- A^+(\zeta^-,y_\perp)}\mathcal{P}e^{-ig\int_{\infty}^{y^-+R^-}d\zeta^- A^+(r_\perp+y_\perp,\zeta^-)}]_{ij}[\mathcal{P}e^{-ig\int_{y^-+R^-}^{\infty}d\zeta^- A^+(\zeta^-,y_\perp)}\mathcal{P}e^{-ig\int_{\infty}^{y^-+R^-}d\zeta^- A^+(r_\perp+y_\perp,\zeta^-)}]^\dagger_{lm}\rangle \\ &= \frac{1}{N_c}[1 - e^{-N_c\Theta(r_\perp^2)\int_{R^-+y^-}^{\infty}d\zeta^-\lambda_A(\zeta^-)}]\delta_{im}\delta_{jl} + e^{-N_c\Theta(r_\perp^2)\int_{R^-+y^-}^{\infty}d\zeta^-\lambda_A(\zeta^-)}\delta_{ij}\delta_{lm},\end{aligned} \tag{40}$$

where i, j, l, and m are color indices. It is worthwhile to mention that two different topologies show up as illustrated in Fig. 2. The gauge links $U^{[-]}$ and $U^{[+]}$ have also been calculated in the previous section. Inserting these results into Eq. (39), one obtains

$$\begin{aligned}\mathcal{M}_A(x,\vec{k}_\perp) = \int \frac{dr^- d^2r_\perp}{(2\pi)^3} e^{ixP^+r^- - i\vec{k}_\perp\cdot\vec{r}_\perp}\int dy^- d^2y_\perp \rho_N^A(y^-)\Big\{&\langle N|\bar{\psi}(0^-,0_\perp)\frac{9}{8}\bar{U}^{[+]}\frac{\mathrm{Tr}_c[\bar{U}^{[\Box]\dagger}]}{N_c}\psi(r^-,r_\perp)|N\rangle \\ &\times e^{-\Theta(r_\perp^2)[C_F\int_{-\infty}^{y^--R^-}d\zeta^-\lambda_A(\zeta^-) + N_c\int_{y^-+R^-}^{\infty}d\zeta^-\lambda_A(\zeta^-)]} \\ &+ \langle N|\bar{\psi}(0^-,0_\perp)\frac{1}{8}\bar{U}^{[-]}\psi(r^-,r_\perp)|N\rangle e^{-C_F\Theta(r_\perp^2)\int_{-\infty}^{y^--R^-}d\zeta^-\lambda_A(\zeta^-)}[1 - e^{-N_c\Theta(r_\perp^2)\int_{y^-+R^-}^{\infty}d\zeta^-\lambda_A(\zeta^-)}] \\ &- \langle N|\bar{\psi}(0^-,0_\perp)\frac{1}{8}\bar{U}^{[-]}\psi(r^-,r_\perp)|N\rangle e^{-C_F\Theta(r_\perp^2)\int_{-\infty}^{y^--R^-}d\zeta^-\lambda_A(\zeta^-)}\Big\}.\end{aligned} \tag{41}$$

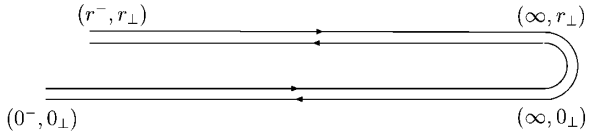

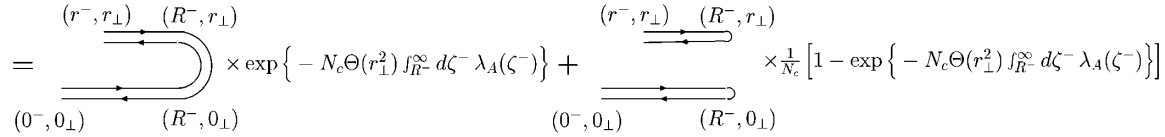

FIG. 2. The gauge link $U^{[+]}U^{[+]\dagger}$ is reduced to two short ones with different color structures by evaluating part of the gauge link stretching from R^- to ∞ in the MV model, where R^- is the radius of a nucleon.

The short Wilson loop appearing in the above equation consists of a short future-pointing and a short past-pointing gauge link: $\bar{U}^{[\Box]} = \bar{U}^{[+]}\bar{U}^{[-]\dagger}$. By approximating the large nucleus as a homogenous system of color sources, we are able to carry out the integration over y^- and $y_\perp$. One then ends up with

$$\mathcal{M}_A(x,\vec{k}_\perp) = \int \frac{dr^- d^2r_\perp}{(2\pi)^3} e^{ixP^+r^- - i\vec{k}_\perp\cdot\vec{r}_\perp} \mathcal{A}\langle N|\bar{\psi}(0^-,0_\perp)\left\{\frac{9}{8}\bar{U}^{[+]}\frac{\mathrm{Tr}_c[\bar{U}^{[\Box]\dagger}]}{N_c} - \frac{1}{8}\bar{U}^{[-]}\right\}\psi(r^-,r_\perp)|N\rangle\left[\frac{e^{\frac{-Q_s^2 r_\perp^2}{4}} - e^{-\frac{Q_{s,q}^2 r_\perp^2}{4}}}{(Q_{s,q}^2 - Q_s^2)r_\perp^2/4}\right], \tag{42}$$

where $Q_s^2 = \alpha_s N_c \ln\frac{1}{r_\perp^2\Lambda_{\mathrm{QCD}}^2}\int_{-\infty}^{\infty} d\zeta^- \lambda_A(\zeta^-)$ is the gluon saturation momentum. To arrive at the above equation, we have made one further approximation, $\int_{-\infty}^{y^- - R^-} d\zeta^-\lambda_A(\zeta^-) + \int_{y^-+R^-}^{\infty} d\zeta^-\lambda_A(\zeta^-) \approx \int_{-\infty}^{\infty} d\zeta^-\lambda_A(\zeta^-)$, which is valid for a large nucleus. One can readily transform this expression to momentum space,

$$\mathbf{f}_{1,q\bar{q}\to\gamma g}(x,k_\perp) = \mathcal{A}\int d^2l_\perp f_{1,q\bar{q}\to\gamma g}(x,l_\perp)\mathcal{F}_{q\bar{q}\to\gamma g}(|\vec{k}_\perp - \vec{l}_\perp|), \tag{43}$$

$$\mathbf{h}^\perp_{1,q\bar{q}\to\gamma g}(x,k_\perp) = \mathcal{A}\int d^2l_\perp(\hat{k}_\perp\cdot\hat{l}_\perp)h^\perp_{1,q\bar{q}\to\gamma g}(x,l_\perp)\mathcal{F}_{q\bar{q}\to\gamma g}(|\vec{k}_\perp - \vec{l}_\perp|), \tag{44}$$

with $\mathcal{F}_{q\bar{q}\to\gamma g}(k_\perp)$ being given by

$$\mathcal{F}_{q\bar{q}\to\gamma g}(|\vec{k}_\perp - \vec{l}_\perp|) = \int\frac{d^2r_\perp}{(2\pi)^2} e^{-i(\vec{k}_\perp - \vec{l}_\perp)\cdot\vec{r}_\perp}\frac{e^{\frac{-Q_s^2 r_\perp^2}{4}} - e^{\frac{-Q_{s,q}^2 r_\perp^2}{4}}}{(Q_{s,q}^2 - Q_s^2)r_\perp^2/4}. \tag{45}$$

Correspondingly, the $k_\perp$ moment of nuclear TMDs read

$$\int d^2k_\perp k_\perp^2 \mathbf{f}_{1,q\bar{q}\to\gamma g}(x,k_\perp) = \mathcal{A}\int d^2l_\perp l_\perp^2 f_{1,q\bar{q}\to\gamma g}(x,l_\perp) + \left[\frac{1}{2}Q_{s,q}^2 + \frac{1}{2}Q_s^2\right]\mathcal{A}f_1(x), \tag{46}$$

$$\int d^2k_\perp k_\perp \mathbf{h}^\perp_{1,q\bar{q}\to\gamma g}(x,k_\perp) = \mathcal{A}\int d^2l_\perp l_\perp h^\perp_{1,q\bar{q}\to\gamma g}(x,l_\perp) = -2\pi M_N\mathcal{A}\frac{N_c^2+1}{N_c^2-1}T_F^{(\sigma)}(x,x), \tag{47}$$

where the nontrivial color factor $(N_c^2+1)/(N_c^2-1)$ originates from the T-odd nature of the quark Boer-Mulders distribution. In the semihard region where the imbalance of the photon-jet produced in pA collisions is of the order $Q_s \gg \Lambda_{\mathrm{QCD}}$, after neglecting the terms suppressed by the power of $\Lambda_{\mathrm{QCD}}^2/Q_s^2$, we have

$$\mathbf{f}_{1,q\bar{q}\to\gamma g}(x,k_\perp) \simeq \mathcal{A}f_1(x)\mathcal{F}_{q\bar{q}\to\gamma g}(k_\perp), \tag{48}$$

$$\mathbf{h}^\perp_{1,q\bar{q}\to\gamma g}(x,k_\perp) \simeq \mathcal{A}2\pi M_N\frac{N_c^2+1}{N_c^2-1}T_F^{(\sigma)}(x,x)\frac{1}{2}\frac{\partial\mathcal{F}_{q\bar{q}\to\gamma g}(k_\perp)}{\partial k_\perp}. \tag{49}$$

The nuclear quark Boer-Mulders function can manifest itself through $\cos 2\phi$ asymmetries as can be seen by convoluting with the function $T_F^{(\sigma)}$ from the proton side. Moreover, if the incoming proton is transversely polarized, the quark Boer-Mulders function can couple with the transversity distribution of the proton and give rise to the single transverse spin asymmetry. Such an observable in pA collisions was also studied from different points of view in the papers [54–57].

Photon-jet pair can also be produced through three other channels: $\bar{q}q \to \gamma g$, $qg \to \gamma q$, and $gq \to \gamma q$. The associated nuclear TMDs contain different gauge link structures in the different channels. By evaluating the gauge links in the MV model, it is straightforward to establish the relations between nucleon TMDs and nuclear TMDs in these processes. However, for simplicity, we only list the $k_\perp$ momenta of the corresponding nuclear TMDs,

$$\int d^2k_\perp k_\perp^2 \bar{\mathbf{f}}_{1,\bar{q}q\to\gamma g}(x,k_\perp) = \mathcal{A}\int d^2l_\perp l_\perp^2 \bar{f}_{1,\bar{q}q\to\gamma g}(x,l_\perp) + \left[\frac{1}{2}Q_{s,q}^2 + \frac{1}{2}Q_s^2\right]\mathcal{A}\bar{f}_1(x), \tag{50}$$

$$\int d^2k_\perp k_\perp^2 \mathbf{f}_{1,qg\to\gamma q}(x,k_\perp) = \mathcal{A}\int d^2l_\perp l_\perp^2 f_{1,qg\to\gamma q}(x,l_\perp) + \left[\frac{1}{2}Q_{s,q}^2 + \frac{1}{2}Q_s^2\right]\mathcal{A}f_1(x), \tag{51}$$

$$\int d^2k_\perp k_\perp^2 \mathbf{G}_{gq\to\gamma q}(x,k_\perp) = \mathcal{A}\int d^2l_\perp l_\perp^2 G_{gq\to\gamma q}(x,l_\perp) + Q_{s,q}^2 \mathcal{A}G(x), \quad (52)$$

where $\bar{\mathbf{f}}_1$ denotes the antiquark distribution.

The average squared transverse momentum imbalance is given by

$$\langle q_\perp^2\rangle = \left(\int d^2q_\perp q_\perp^2 \frac{d\sigma}{d\mathcal{P}.\mathcal{S}.d^2q_\perp}\right)\Big/\frac{d\sigma}{d\mathcal{P}.\mathcal{S}.}, \quad (53)$$

where $d\mathcal{P}.\mathcal{S}. = dy_1 dy_2 d^2p_\perp$ stands for the phase space with y_1, y_2 being the produced photon and jet rapidities, respectively. The nuclear broadening of the photon-jet imbalance is defined as

$$\Delta\langle q_\perp^2\rangle = \langle q_\perp^2\rangle_{pA} - \langle q_\perp^2\rangle_{pp}. \quad (54)$$

Putting all these together, within the TMD factorization framework the nuclear enhancement of the photon-jet squared transverse momentum imbalance is given by

$$\Delta\langle q_\perp^2\rangle = \Delta\langle k_\perp^2\rangle = \frac{1}{2}Q_{s,q}^2 + \frac{1}{2}Q_s^2 - \frac{[\frac{1}{2}Q_s^2 - \frac{1}{2}Q_{s,q}^2]\Sigma_a H^a_{gq\to\gamma q}}{\Sigma_a[H^a_{qg\to\gamma q} + H^a_{gq\to\gamma q} + H^a_{q\bar{q}\to\gamma g} + H^a_{\bar{q}q\to\gamma g}]}, \quad (55)$$

where a runs all quark flavors. The partonic hard scattering differential cross sections read [58]

$$H^a_{qg\to\gamma q} = e_q^2\frac{1}{N_c}\left(-\frac{\hat{s}}{\hat{t}} - \frac{\hat{t}}{\hat{s}}\right)\mathbf{f}_1^q(x)G(x'), \quad (56)$$

$$H^a_{gq\to\gamma q} = e_q^2\frac{1}{N_c}\left(-\frac{\hat{s}}{\hat{u}} - \frac{\hat{u}}{\hat{s}}\right)\mathbf{G}(x)f_1^a(x'), \quad (57)$$

$$H^a_{q\bar{q}\to\gamma g} = e_q^2\frac{N_c^2-1}{N_c^2}\left(\frac{\hat{t}}{\hat{u}} + \frac{\hat{u}}{\hat{t}}\right)\mathbf{f}_1^a(x)\bar{f}_1^a(x'), \quad (58)$$

$$H^a_{\bar{q}q\to\gamma g} = e_q^2\frac{N_c^2-1}{N_c^2}\left(\frac{\hat{t}}{\hat{u}} + \frac{\hat{u}}{\hat{t}}\right)\bar{\mathbf{f}}_1^a(x)f_1^a(x'). \quad (59)$$

Here, $\hat{s}$, $\hat{u}$, and $\hat{t}$ are the usual partonic Mandelstam variables. The collinear momentum fraction is fixed by the kinematical constraint,

$$x' = \frac{p_\perp}{\sqrt{s}}(e^{y_1} + e^{y_2}), \qquad x' = \frac{p_\perp}{\sqrt{s}}(e^{-y_1} + e^{-y_2}), \quad (60)$$

where $s = (P + P')^2$ is the center-of-mass energy squared. By noticing $Q_s^2 = \frac{C_A}{C_F}Q_{s,q}^2$, the nuclear broadening of the photon-jet imbalance varies from $1\frac{5}{8}Q_{s,q}^2$ to $Q_{s,q}^2$ depending on the specific kinematical variables.

B. $k_\perp$ broadening in heavy quark pair production

Quark-antiquark pair production in high energy pA collisions is dominated by the gluon initiated parton subprocess,

$$g_p(x_1P') + g_A(x_2P) \to Q(p_1) + \bar{Q}(p_2). \quad (61)$$

The nuclear enhancement of the quark pair transverse momentum imbalance $\vec{q}_\perp = \vec{p}_{1\perp} + \vec{p}_{2\perp}$ is directly sensitive to nuclear gluon TMD distributions. The color flow in this subprocess is more complicated than that for photon-jet production in pA collisions. The nuclear gluon TMDs associated with different Feynman diagrams contain different gauge link structures. Here we show two examples:

$$\mathcal{M}_A^a \propto \langle A|\mathrm{Tr_c}\left[F_{+\perp}\left\{\frac{9}{8}\frac{\mathrm{Tr_c}[U^{[\square]\dagger}]}{N_c}U^{[-]\dagger} - \frac{1}{8}U^{[+]\dagger}\right\}F_{+\perp}U^{[+]}\right]|A\rangle, \quad (62)$$

$$\mathcal{M}_A^e \propto \langle A|\mathrm{Tr_c}\left[F_{+\perp}U^{[-]\dagger}F_{+\perp}U^{[+]}\right]\frac{\mathrm{Tr_c}[U^{[\square]\dagger}]}{N_c} - \frac{1}{N_c}\mathrm{Tr_c}[\mathrm{F}_{+\perp}U^{[\square]\dagger}]\,\mathrm{Tr_c}[\mathrm{F}_{+\perp}U^{[\square]}]|A\rangle, \quad (63)$$

where gauge links appearing in $\mathcal{M}_A^a$ and $\mathcal{M}_A^e$ originate from initial/final state interactions in the Feynman diagrams Figs. 3(a) and 3(e), respectively. All other gauge links appearing in this hard scattering process are given in [25]. One can compute the transverse momentum spectrum of the gluon distribution associated with each Feynman diagram following a similar method as introduced in the previous subsections. With the derived nuclear gluon TMDs, we obtain

$$\int d^2k_\perp k_\perp^2 \mathbf{G}^a_{gg\to Q\bar{Q}}(x,k_\perp) = \mathcal{A}\int d^2l_\perp l_\perp^2 G^a_{gg\to Q\bar{Q}}(x,l_\perp) + \left[1 - \frac{1}{2}\frac{1}{N_c^2-1}\right]Q_s^2\mathcal{A}G(x), \quad (64)$$

$$\int d^2k_\perp k_\perp^2 \mathbf{G}^b_{gg\to Q\bar{Q}}(x,k_\perp) = \mathcal{A}\int d^2l_\perp l_\perp^2 G^b_{gg\to Q\bar{Q}}(x,l_\perp) + \left[1 - \frac{1}{2}\frac{1}{N_c^2-1}\right]Q_s^2\mathcal{A}G(x), \quad (65)$$

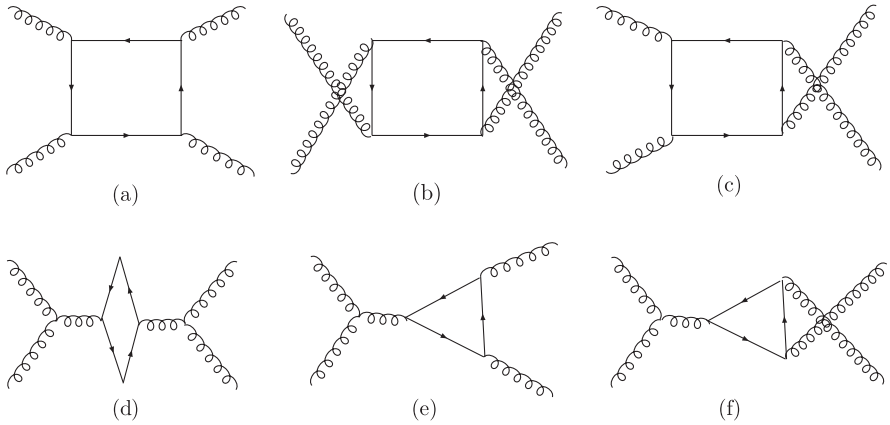

FIG. 3. Feynman diagrams contributing to quark-antiquark pair production.

$$\int d^2k_\perp k_\perp^2 \mathbf{G}^c_{gg\to Q\bar{Q}}(x,k_\perp) = \mathcal{A}\int d^2l_\perp l_\perp^2 G^c_{gg\to Q\bar{Q}}(x,l_\perp) + \frac{3}{2}Q_s^2\mathcal{A}G(x), \tag{66}$$

$$\int d^2k_\perp k_\perp^2 \mathbf{G}^d_{gg\to Q\bar{Q}}(x,k_\perp) = \mathcal{A}\int d^2l_\perp l_\perp^2 G^d_{gg\to Q\bar{Q}}(x,l_\perp) + Q_s^2\mathcal{A}G(x), \tag{67}$$

$$\int d^2k_\perp k_\perp^2 \mathbf{G}^e_{gg\to Q\bar{Q}}(x,k_\perp) = \mathcal{A}\int d^2l_\perp l_\perp^2 G^e_{gg\to Q\bar{Q}}(x,l_\perp) + Q_s^2\mathcal{A}G(x), \tag{68}$$

$$\int d^2k_\perp k_\perp^2 \mathbf{G}^f_{gg\to Q\bar{Q}}(x,k_\perp) = \mathcal{A}\int d^2l_\perp l_\perp^2 G^f_{gg\to Q\bar{Q}}(x,l_\perp) + Q_s^2\mathcal{A}G(x). \tag{69}$$

It is easy to verify that the hard coefficient computed from the Feynman diagram Fig. 3(c) is suppressed by the factor of $1/N_c^2$ as compared to the contributions from other diagrams in the large N_c limit. Thus, we conclude that the nuclear $k_\perp$ broadening for quark-anitquark pair production in pA collisions is Q_s^2 in the large N_c limit.

IV. PHENOMENOLOGY APPLICATIONS

In this section, we discuss phenomenology applications of our results and compare our formalism with the higher twist collinear approach. We start from numerically evaluating nuclear $k_\perp$ broadening for jet production in eA collisions. The analytical result for this observable takes a simple form,

$$\Delta\langle k_\perp^2\rangle_{\gamma^* q\to q} = Q_{s,q}^2/2. \tag{70}$$

However, in deriving the above result, we only took into account the contributions to the gauge link from color sources outside of the nucleon to which the struck parton belongs. To remedy this problem, the above equation should be slightly modified as follows:

$$\Delta\langle k_\perp^2\rangle_{\gamma^* q\to q} = \frac{\mathcal{A}^{1/3}-1}{\mathcal{A}^{1/3}}Q_{s,q}^2/2, \tag{71}$$

where we adopt the parametrization for the saturation momentum used in the GBW model [59]: $Q_s^2 = \mathcal{A}^{1/3}Q_0^2(x_0/x_g)^\lambda$ with $Q_0^2 = 1\ \mathrm{GeV}^2$, $x_0 = 3\times 10^{-4}$, and $\lambda \approx 0.3$. For lead or gold targets, $\mathcal{A}^{1/3}-1$ is approximately equal to 5.

The natural next step is to fix x_g. At first glance, gluons building up gauge links carry exactly zero longitudinal momentum due to the contour integration around the gluon pole $1/(x_g - i\epsilon)$ (for final state interactions). This pole arises when performing the calculation in the collinear approximation. However, if one keeps the gluon transverse momentum $k_{g\perp}$, the gluon pole in jet production in the SIDIS process will be modified to

$$\frac{1}{x_g - k_{g\perp}^2/(2p\cdot q) - i\epsilon}, \tag{72}$$

where q is the virtual photon momentum. Within the leading logarithm accuracy, it is convenient to replace $k_{g\perp}^2$ in the above formula by $\Delta\langle k_\perp^2\rangle$. Once x_g is fixed as $\Delta\langle k_\perp^2\rangle/(2p\cdot q)$, one obtains (for a lead or gold target)

$$\begin{aligned}\Delta\langle k_\perp^2\rangle_{\gamma^* q\to q} &= \left[\frac{1}{2}\frac{C_F}{C_A}(\mathcal{A}^{1/3}-1)Q_0^2\right]^{1/(1+\lambda)}\left(s\frac{x_0}{1+x_B}\right)^{\lambda/(1+\lambda)}\\ &\approx 1.08\left(s\frac{x_0}{1+x_B}\right)^{0.23}(Q_0^2)^{0.77},\end{aligned} \tag{73}$$

where $s = (p+q)^2$ and $x_B \equiv Q^2/2p\cdot q = Q^2/(s+Q^2)$ with $Q^2 = -q^2$ being the virtual photon virtuality. The above equation holds as long as x_B is of the order of 1 and $x_g \le 0.01$ where the MV model can apply. This implies

that our formalism is invalid at relatively low energy [60]. Given $x_B = 0.2$ and $\sqrt{s} = 35$ GeV accessible at a future EIC, the nuclear $k_\perp$ broadening for jet production in the SIDIS process gives $\Delta\langle k_\perp^2\rangle_{\gamma^* q\to q} \approx 0.82$ GeV^2. For the Drell-Yan process one can fix the saturation scale in the same way. Unfortunately, we are not able to unambiguously determine the saturation scale for other processes.

Now we compare our result with that obtained from the higher twist collinear approach. As mentioned in the introduction, the process dependent $k_\perp$ broadening effect was also investigated within the higher twist collinear factorization framework [33,34] which can be applied in the intermediate or large x region. In this formalism, the effect of initial/final state multiple scattering generating $k_\perp$ broadening is encoded in the collinear twist-4 quark-gluon correlation functions $T^{(I)}_{q,g/A}(x)$ and $T^{(F)}_{q,g/A}(x)$. These functions are parametrized as follows:

$$\frac{4\pi^2\alpha_s}{N_c} T^{(I)}_{q,g/A}(x) = \frac{4\pi^2\alpha_s}{N_c} T^{(F)}_{q,g/A}(x) = \xi^2(\mathcal{A}^{1/3} - 1) f_{q,g/A}(x), \quad (74)$$

where ξ^2 represents a characteristic scale of parton multiple scattering, and $f_{q,g/A}(x)$ is the standard leading-twist parton distribution function for quarks and gluons, respectively. If we identify the saturation scale as

$$\frac{1}{2}\frac{Q^2_{s,q}}{C_F} = \frac{1}{2}\frac{Q_s^2}{C_A} = \xi^2 \mathcal{A}^{1/3}, \quad (75)$$

our analytical results for $k_\perp$ broadening take the same form as those presented in [33,34]. In [33,34], ξ^2 is chosen to be 0.12 GeV^2. Provided that one evaluates the saturation scale using the same value $\xi^2 = 0.12$ GeV^2, we a have numerical result for jet $k_\perp$ broadening in SIDIS $\Delta\langle k_\perp^2\rangle_{\gamma^* q\to q} = 0.8$ GeV^2, which is very close to that calculated with the GBW parametrization. We would also get the identical numerical results for all other processes using Eq. (75).

Apart from the process dependent unpolarized nuclear TMDs, the process dependent nuclear quark Boder-Mulders function is also studied in this paper. Below we discuss the corresponding phenomenological implications for the polarized cases. In both SIDIS and DY in pA collisions, the nuclear quark Boer-Mulders function can give rise to $\cos 2\phi$ azimuthal asymmetries by coupling with the Collins fragmentation function and the antiquark Boer-Mulders function from the proton side [61], respectively. According to our calculation, in the semihard region, the transverse momentum dependence of the asymmetry is unambiguously determined by the ratio

$$\langle\cos 2\phi\rangle(k_\perp) \propto \frac{\partial \mathcal{F}_{\rm DIS}(k_\perp)}{\partial k_\perp} \Big/ \mathcal{F}_{\rm DIS}(k_\perp).$$

Such observables can in principle be measured in unpolarized eA collisions at EIC and unpolarized pA collisions at RHIC. We leave detailed phenomenological studies for a future work.

V. SUMMARY

We have established relations between nuclear TMDs and the corresponding nucleon ones by computing contributions from the process dependent gauge links in the MV model. In particular, in the semihard region where quark transverse momenta are of the order of the saturation scale, unpolarized nuclear TMDs are determined by the process dependent small x gluon distributions, while nuclear quark Boer-Mulders distributions are expressed as products of $T_F^{(\sigma)}(x, x)$ and the differential of the same gluon distributions with respect to gluon transverse momentum. We stress again that the formalism developed in this paper applies only for nuclear TMDs at intermediate or large x.

Two phenomenological applications of our work are nuclear $k_\perp$ broadening and the $k_\perp$ dependence of the asymmetries generated by the quark Boer-Mulders function in eA and pA collisions. To be more specific, we calculated nuclear $k_\perp$ broadening for jet and dijet production in eA collisions, and the nuclear enhancement of the transverse momentum imbalance for Drell-Yan lepton pair production, photon-jet production, and quark-antiquark pair production in pA collisions. To investigate how the quark Boer-Mulders function are affected by the surrounding cold nuclear matter, we also proposed to measure $\cos 2\phi$ azimuthal asymmetries in SIDIS off a large nucleus and Drell-Yan pairs in pA collisions. It will be interesting to test our predications at RHIC and the planned EIC.

ACKNOWLEDGMENTS

This work has been supported by BMBF (OR 06RY9191 and 05P12WRFTE).

[1] G. T. Bodwin, S. J. Brodsky, and G. P. Lepage, Phys. Rev. Lett. **47**, 1799 (1981); Phys. Rev. D **39**, 3287 (1989).
[2] M. Luo, J.-w. Qiu, and G. F. Sterman, Phys. Lett. B **279**, 377 (1992); Phys. Rev. D **49**, 4493 (1994); **50**, 1951 (1994).
[3] R. J. Fries, Phys. Rev. D **68**, 074013 (2003).
[4] A. Majumder and B. Muller, Phys. Rev. C **77**, 054903 (2008).
[5] J. Dolejsi, J. Hufner, and B. Z. Kopeliovich, Phys. Lett. B **312**, 235 (1993).

[6] M. B. Johnson, B. Z. Kopeliovich, and A. V. Tarasov, Phys. Rev. C **63**, 035203 (2001).
[7] R. Baier, Y. L. Dokshitzer, A. H. Mueller, S. Peigne, and D. Schiff, Nucl. Phys. **B484**, 265 (1997).
[8] B. Wu, J. High Energy Phys. 10 (2011) 029.
[9] T. Liou, A. H. Mueller, and B. Wu, Nucl. Phys. **A916**, 102 (2013).
[10] M. Gyulassy, P. Levai, and I. Vitev, Phys. Rev. D **66**, 014005 (2002).
[11] A. Dumitru and J. Jalilian-Marian, Phys. Lett. B **547**, 15 (2002).
[12] D. Kharzeev, Y. V. Kovchegov, and K. Tuchin, Phys. Rev. D **68**, 094013 (2003).
[13] Z. T. Liang, X. N. Wang, and J. Zhou, Phys. Rev. D **77**, 125010 (2008).
[14] A. Idilbi and A. Majumder, Phys. Rev. D **80**, 054022 (2009).
[15] F. D'Eramo, H. Liu, and K. Rajagopal, Phys. Rev. D **84**, 065015 (2011).
[16] G. Ovanesyan and I. Vitev, J. High Energy Phys. 06 (2011) 080.
[17] M. Benzke, N. Brambilla, M. A. Escobedo, and A. Vairo, J. High Energy Phys. 02 (2013) 129.
[18] J. Casalderrey-Solana and X.-N. Wang, Phys. Rev. C **77**, 024902 (2008).
[19] A. H. Mueller and S. Munier, Nucl. Phys. **A893**, 43 (2012).
[20] J. C. Collins and D. E. Soper, Nucl. Phys. **B193**, 381 (1981); **B213**, 545(E) (1983); **B194**, 445 (1982).
[21] X. D. Ji, J. P. Ma, and F. Yuan, Phys. Rev. D **71**, 034005 (2005).
[22] J.-H. Gao, Z.-t. Liang, and X.-N. Wang, Phys. Rev. C **81**, 065211 (2010).
[23] Y.-k. Song, J.-h. Gao, Z.-t. Liang, and X.-N. Wang, Phys. Rev. D **83**, 054010 (2011).
[24] J.-H. Gao, A. Schafer, and J. Zhou, Phys. Rev. D **85**, 074027 (2012).
[25] C. J. Bomhof, P. J. Mulders, and F. Pijlman, Phys. Lett. B **596**, 277 (2004); Eur. Phys. J. C **47**, 147 (2006).
[26] B.-W. Xiao and F. Yuan, Phys. Rev. Lett. **105**, 062001 (2010); Phys. Rev. D **82**, 114009 (2010).
[27] F. Dominguez, B. W. Xiao, and F. Yuan, Phys. Rev. Lett. **106**, 022301 (2011).
[28] F. Dominguez, C. Marquet, B. W. Xiao, and F. Yuan, Phys. Rev. D **83**, 105005 (2011).
[29] A. Metz and J. Zhou, Phys. Rev. D **84**, 051503 (2011).
[30] E. Akcakaya, A. Schafer, and J. Zhou, Phys. Rev. D **87**, 054010 (2013).
[31] T. C. Rogers and P. J. Mulders, Phys. Rev. D **81**, 094006 (2010).
[32] Z.-B. Kang and J.-W. Qiu, Phys. Rev. D **77**, 114027 (2008); Phys. Lett. B **721**, 277 (2013).
[33] Z.-B. Kang, I. Vitev, and H. Xing, Phys. Rev. D **85**, 054024 (2012).
[34] H. Xing, Z.-B. Kang, I. Vitev, and E. Wang, Phys. Rev. D **86**, 094010 (2012).
[35] L. D. McLerran and R. Venugopalan, Phys. Rev. D **49**, 2233 (1994); **49**, 3352 (1994).
[36] J. Jalilian-Marian, A. Kovner, L. D. McLerran, and H. Weigert, Phys. Rev. D **55**, 5414 (1997).
[37] D. Boer and P. J. Mulders, Phys. Rev. D **57**, 5780 (1998).
[38] J. Zhou, F. Yuan, and Z.-T. Liang, Phys. Rev. D **78**, 114008 (2008).
[39] J. Zhou, F. Yuan, and Z.-T. Liang, Phys. Rev. D **81**, 054008 (2010).
[40] J. Zhou, F. Yuan, and Z.-T. Liang, Phys. Lett. B **678**, 264 (2009).
[41] X. D. Ji and F. Yuan, Phys. Lett. B **543**, 66 (2002); A. V. Belitsky, X. Ji, and F. Yuan, Nucl. Phys. **B656**, 165 (2003).
[42] E. Iancu, A. Leonidov, and L. McLerran, arXiv:hep-ph/0202270.
[43] B. U. Musch, P. Hagler, M. Engelhardt, J. W. Negele, and A. Schafer, Phys. Rev. D **85**, 094510 (2012).
[44] D. Boer, P. J. Mulders, and F. Pijlman, Nucl. Phys. **B667**, 201 (2003).
[45] J. Jalilian-Marian and Y. V. Kovchegov, Prog. Part. Nucl. Phys. **56**, 104 (2006).
[46] S. J. Brodsky, D. S. Hwang, and I. Schmidt, Phys. Lett. B **530**, 99 (2002).
[47] J. C. Collins, Phys. Lett. B **536**, 43 (2002).
[48] P. J. Mulders and J. Rodrigues, Phys. Rev. D **63**, 094021 (2001).
[49] M. Anselmino, M. Boglione, U. D'Alesio, E. Leader, S. Melis, and F. Murgia, Phys. Rev. D **73**, 014020 (2006); S. Meissner, A. Metz, and K. Goeke, Phys. Rev. D **76**, 034002 (2007).
[50] F. Dominguez, J.-W. Qiu, B.-W. Xiao, and F. Yuan, Phys. Rev. D **85**, 045003 (2012).
[51] A. Schafer and J. Zhou, Phys. Rev. D **85**, 114004 (2012).
[52] T. Liou, Nucl. Phys. **A897**, 122 (2013).
[53] J. P. Blaizot, F. Gelis, and R. Venugopalan, Nucl. Phys. **A743**, 57 (2004).
[54] D. Boer and A. Dumitru, Phys. Lett. B **556**, 33 (2003); D. Boer, A. Dumitru, and A. Hayashigaki, Phys. Rev. D **74**, 074018 (2006); D. Boer, A. Utermann, and E. Wessels, Phys. Lett. B **671**, 91 (2009).
[55] Z.-B. Kang and F. Yuan, Phys. Rev. D **84**, 034019 (2011).
[56] Y. V. Kovchegov and M. D. Sievert, Phys. Rev. D **86**, 034028 (2012); **86**, 079906(E) (2012).
[57] Z.-B. Kang and B.-W. Xiao, Phys. Rev. D **87**, 034038 (2013).
[58] J. F. Owens, Rev. Mod. Phys. **59**, 465 (1987).
[59] K. J. Golec-Biernat and M. Wusthoff, Phys. Rev. D **59**, 014017 (1998).
[60] A. Airapetian *et al.* (HERMES Collaboration), Phys. Lett. B **684**, 114 (2010).
[61] D. Boer, Phys. Rev. D **60**, 014012 (1999).